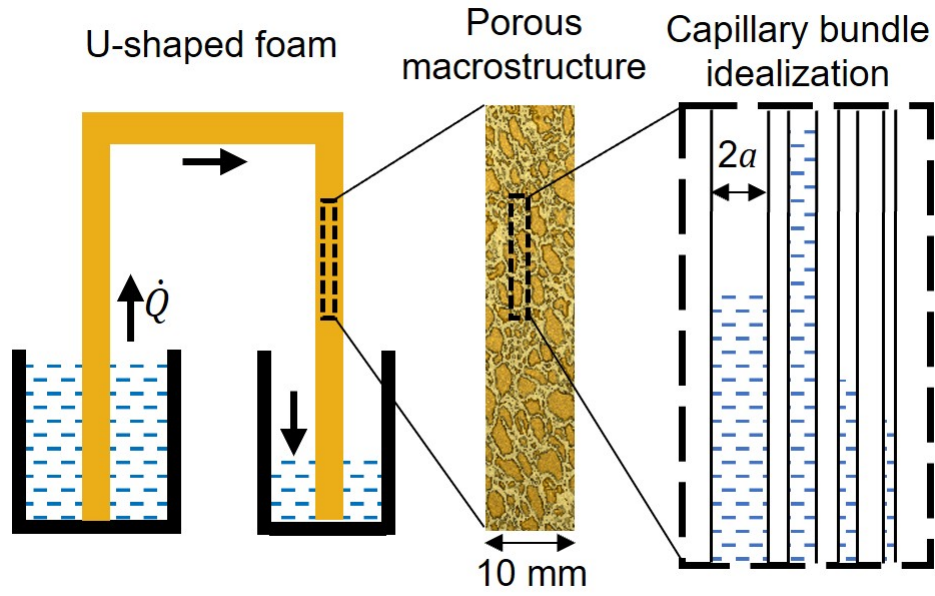


Graphical Abstract

The Transport of Water in a Cellulose Foam

Ratul Das, Vikram S. Deshpande, Norman A. Fleck



Highlights

The Transport of Water in a Cellulose Foam

Ratul Das, Vikram S. Deshpande, Norman A. Fleck

- **Critical experiment shows an established capillary flow above the inferred Jurin height for cellulose foam.**
- **Dry cellulose foam is idealised as a bundle of individual capillary tubes of varying radius.**
- **A novel experimental technique is developed in order to estimate the probability density distribution of capillary tube radius.**

The Transport of Water in a Cellulose Foam

Ratul Das^a, Vikram S. Deshpande^a, Norman A. Fleck^{a,*}

^a*Engineering Department, Cambridge University, Trumpington Street, Cambridge, CB2 1PZ, , England*

Abstract

A novel experimental protocol and analysis technique is developed to determine whether water rise in a cellulose foam is by capillary flow alone, or is by capillary flow followed by diffusion. The literature is divided in the interpretation of the water rise versus time characteristic in the foam, and our study suggests that capillary flow dominates. The present study reveals that the foam can be idealised as a spectrum of individual capillary tubes; the probability density function of tube radius is obtained from a systematic set of siphon discharge experiments on inverted U-tubes made from the foam. We show that the capillary tube radii range from 0.1 μm to 100 μm , with two distinct peaks in probability density at 0.5 μm and 10 μm . The nature of the flow within the U-tube is confirmed by interrupting a siphon experiment and measuring the density profile along the length of the inverted U-tube by in-situ X-ray computed tomography. The probability density function is then used to predict the transient rise of water in a vertical column of dry foam.

Keywords: Capillary rise, cellulose foam, porous media

1. Introduction

The absorption and flow of liquids through porous media are common phenomena encountered in daily life, in several branches of science, and in many engineering applications. Porous xylem and phloem plant tissues facilitate water and nutrient transport through plant stems and tree trunks. Porous filters or catalyst beds are commonly used to accelerate or retard chemical reactions [1]. Sponges and paper towels are used to soak up water spills and recently, hydrophobic-chemical-coated sponges have been developed to clean up oil spills in oceans [2–4]. Paper-based microfluidics devices μ -PADs are used as inexpensive medical diagnosis tests [5]. Cellulose sponges are also used in medical implants, and for dressings

*Corresponding author

Email address: naf1@cam.ac.uk (Norman A. Fleck)

to promote wound healing [6, 7]. Thus, the flow of liquid through porous media is both ubiquitous and of practical use. The present study focuses on water migration in cellulose foam.

Cellulose foams can behave as actuating soft solids, such that the addition of water to a dry, pre-compressed foam leads to one-way, one-dimensional actuation, as reported by Mirzajanzadeh et al. [8]. To achieve such an actuation event, the foam is first conditioned in the wet state by compressing it along the rise direction of the foam. The foam is then dried in the compressed state, resulting in the stable pre-triggered state. Upon addition of water to the dry, pre-compressed foam it re-expands in the rise direction by a stretch factor on the order of $\times 10$: this is the actuation event. The details of the mechanism of fluid imbibition in the pre-compressed and post-actuation state need to be resolved in order to build up a full micro-mechanical model of the actuation response of the cellulose foam. The present study is the first step in achieving this: it gives an experimental protocol and accompanying analysis to determine the mechanism of fluid flow within cellulose foam in the actuated state.

Cellulose open-cell foam comprises an interconnected network of millimetre-scale voids in a cellulose sheet containing micropores of diameter $1\ \mu\text{m}$ to $10\ \mu\text{m}$. Consequently, it can soak up and retain a large quantity of water or non-aqueous liquids such as ethanol or glycerol. Liquid flow in such porous materials can occur by two distinct mechanisms: (i) pressure-driven capillary flow through narrow channels [8–10], and (ii) concentration-driven molecular diffusion when a concentration gradient exists in the lattice, along with the possibility of molecular trapping at molecular sites [11–13]. The relative significance of these alternative mechanisms remains controversial, and the purpose of this paper is to report a critical experiment that distinguishes between them for the case of a cellulose foam.

More specifically, the present study extends the recent work of Mirzajanzadeh et al. [11] on the transport of liquid water through a cellulose foam. They suggested that the rise of water from a water-filled reservoir in a vertical column of dry foam is first by capillary flow (termed Stage I) and then by diffusion (Stage II), with a distinct change in the slope of water height h versus time t curve at the transition from Stage I to Stage II (see Figure 1). In contrast, in the present study, the flow of water through a cellulose foam will be idealised by the rise of water up a vertical array of capillary tubes, with a range of diameters.

It is instructive to recall the classical solution for the transient rise of a liquid of density ρ up a capillary tube of diameter $2a$ [14–16]. Denote the liquid viscosity by η , the liquid-air surface tension by γ , the contact angle by ω , and the acceleration due to gravity by g , as shown in Figure 1 (a). At $t = 0$, the bottom of the empty vertical capillary tube is placed in a liquid reservoir. The capillary pressure $2\gamma'/a$ (where $\gamma' = \gamma \cos \omega$) that drives the upward flow of the liquid is balanced by the pressure drop due to viscous losses associated with pipeflow over a length h and by the weight of the liquid column ρgh . Write \dot{h} as the rate of increase of liquid column height with time. Then, the governing equation for $h(t)$ is

$$\frac{8\eta h \dot{h}}{a^2} + \rho gh = \frac{2\gamma'}{a}, \quad (1)$$

with solution

$$h + \frac{2\gamma'}{\rho ga} \ln \left[1 - \frac{\rho ga}{2\gamma'} h \right] = -\frac{\rho ga^2}{8\eta} t, \quad (2)$$

known as the Washburn law. Capillary flow of this type was investigated by Bell and Cameron [15], and Lucas [16] in addition to Washburn [14]. The solution Equation (2) has

an initial regime with the feature that $h(t)$ is independent of the acceleration due to gravity, and is of the form

$$h = \left[\frac{\gamma'at}{2\eta} \right]^{1/2}, \quad (3)$$

The response $h(t)$ then undergoes a sharp transition to a final limiting value of height known as the Jurin height h_J where

$$h_J = \frac{2\gamma'}{\rho ga}, \quad (4)$$

as first obtained by Jurin [17]. The above approach has been extended to capillary tubes of non-circular cross-section such as triangular [18–20] or rectangular [21, 22].

Given this background, Mirzajanzadeh et al. [11] interpreted the height of water-front at which Stage I is superseded by Stage II (recall Figure 1 (b)) as the Jurin height associated with the smallest diameter of capillary tube within the foam. Mirzajanzadeh et al. [11] hypothesized that the continued migration of water above the Jurin height in Stage II is by diffusion within the cell walls of the dry foam. Additional studies in the literature support the notion of two distinct stages of liquid transport in a cellulose foam [8, 9, 23]. Whilst there is broad agreement that capillary flow occurs initially, there is debate on the operative mechanism at a height above the observed Jurin height. For example, Kim et al. [9] and Ha et al. [24] ascribe the flow in Stage II to secondary capillary flow along the corners of millimeter-scale macrovoids, with the capillary pressure set by micropores in the walls of the macrovoids.

We begin our study by reporting a critical siphon discharge experiment on inverted U-

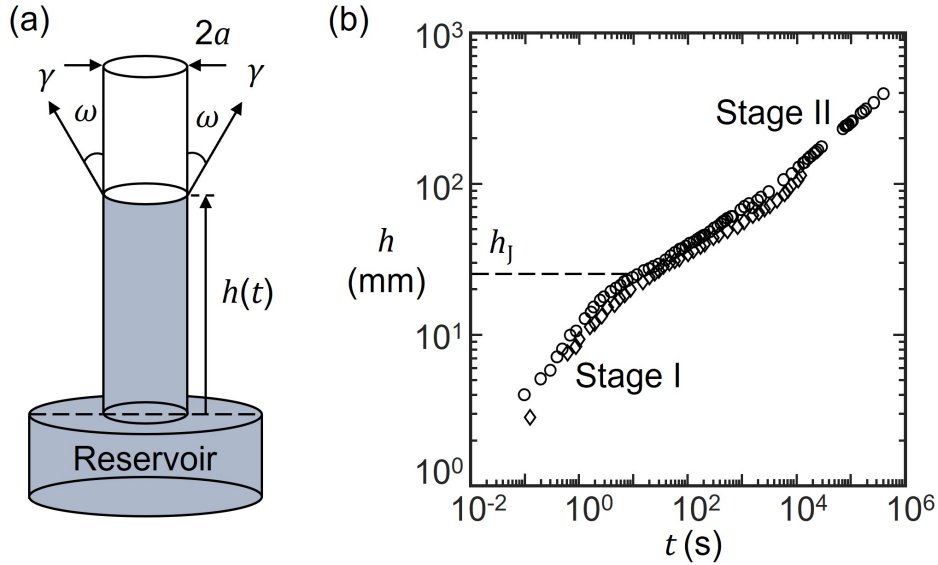


Figure 1: (a) Liquid rise in a capillary tube. (b) Observed water rise $h(t)$ in a vertical column of dry cellulose foam, using data from Mirzajanzadeh et al. [11].

shaped foam specimens to reveal that liquid transport through the foam is by capillary flow and not by concentration-driven diffusion. This implies that Stage II flow is associated with capillary flow in the cell walls of the cellulose foam. A theory of siphon discharge is then developed for capillary tubes with a spectrum of radii. The distribution of capillary radius is deduced from a comprehensive set of siphon discharge experiments, and is then used to predict water rise from a reservoir into a vertical column of dry foam. Such a siphon theory has wide applications, ranging from siphon discharge in porous media for the clean-up of oil spill [25], to the manufacture of potassium ion batteries [26], and to fluid flow in microfluidic devices [27].

2. Critical Experiment on Inverted U-shaped Foam

A critical experiment is reported on the migration of water along an inverted U-shaped foam specimen. The configuration of the experiment is sketched in Figure 2. Concentration

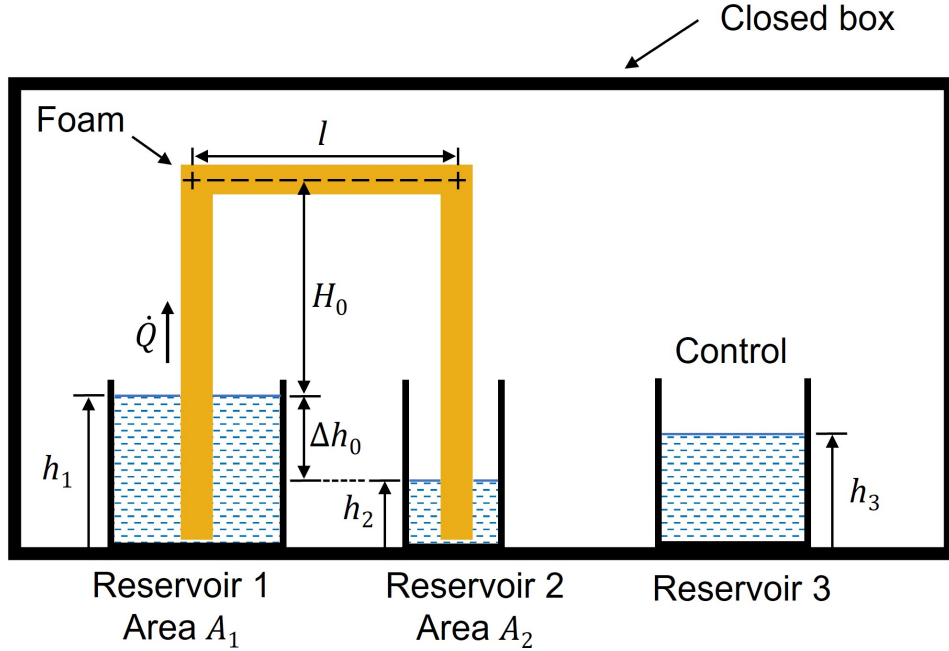


Figure 2: Schematic of siphon discharge experiment from Reservoir 1 to Reservoir 2 via an inverted U-shaped foam.

driven diffusion of water cannot occur in this configuration as a water reservoir exists at each end of the specimen. There remains the possibility of capillary flow if the shorter left arm of the specimen can self-prime as a siphon from the upper Reservoir 1.

Mirzajanzadeh et al. [11] measured the so-called Jurin height of a pre-expanded cellulose foam to be $h_J = 24$ mm. They conjectured that liquid transport above the Jurin height is exclusively by diffusion, driven by the concentration gradient within the cell walls of the foam. If their hypothesis is correct, then capillary rise is excluded and no drainage can occur from the upper Reservoir 1 to a lower Reservoir 2 when the height of the leftmost column of the inverted U-tube exceeds $h_J = 24$ mm. This hypothesis is now tested by measuring the drainage from an upper reservoir to a lower reservoir via an inverted U-tube made from the same foam as that used by Mirzajanzadeh et al. [11]; the height of the shorter left arm now exceeds the Jurin height of $h_J = 24$ mm.

2.1. Material

The cellulose foam is made by first adding sodium sulphate crystals to a liquid viscose solution to define the macro-voids of the liquid foam, and then by dissolving and draining the sodium sulphate crystals at 90 °C to 95 °C [28]. The heating process that dissolves the sodium sulphate crystals also solidifies the liquid cellulose. The wet foam is thermomechanically compressed in one direction and then dried in the compressed state to form a sheet of density $\rho = 680 \text{ kg/m}^3$; its relative density is $\bar{\rho} = 0.45$ compared to that of fully dense cellulose (1500 kg/m^3). The direction of compression during manufacturing defines the Rise Direction. The foam is supplied¹ in the dry, compressed state as rectangular sheets of dimension $420 \text{ mm} \times 300 \text{ mm} \times 2.4 \text{ mm}$. The high porosity of the foam is regenerated by immersing the dry compressed foam in water and then drying it in an oven at 30 °C for 8 hours. The re-expanded foam has a density of 50 kg/m^3 in the dry state, a relative density of $\bar{\rho} = 0.033$, and a thickness of 35 mm. The low relative density is attributed to the presence of millimetre-scale voids (of geometry defined by the sodium sulphate crystals) and micron-scale voids within the cell walls. In the remainder of this study, we refer to the re-expanded cellulose foam simply as cellulose foam.

The microstructure of the cellulose foam, as visualised via a X-Ray computed tomography (XCT), is shown in [Figure 3\(a\)](#). The X-ray scans are performed using an 80 kV X-Ray source with 130 μA operating current in a NIKON XT H 225ST X-Ray Computed Tomography machine. The working distance of the sample from the X-ray source is such that the resolution is set by the voxel size of 90 μm . The network of large millimetre-scale

¹Suvcic Products Limited, 3 Brunel Rd., Totton, Southampton SO40 3WX, United Kingdom.

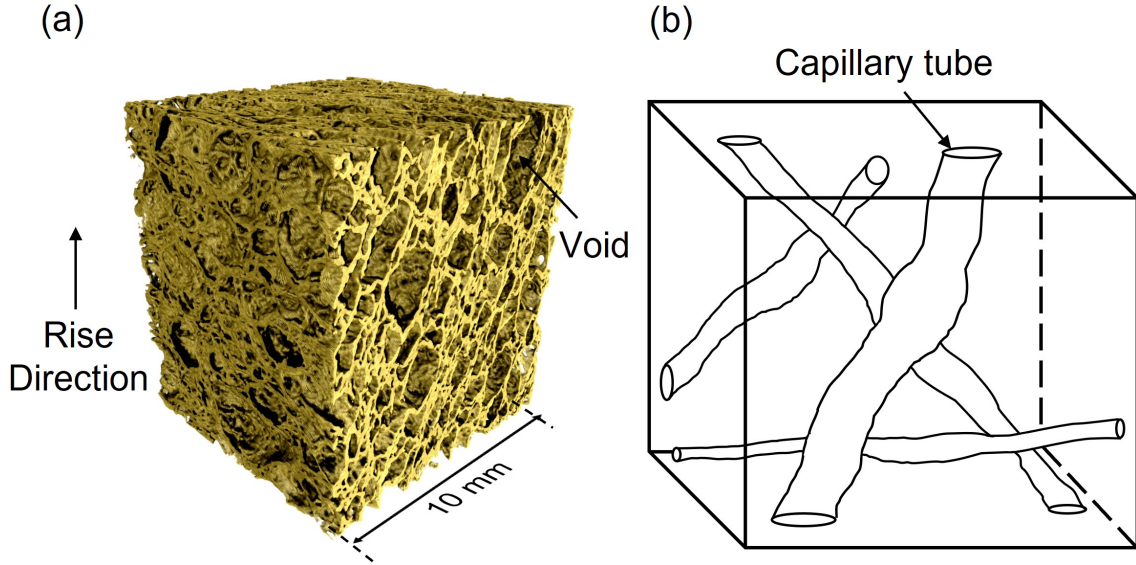


Figure 3: (a) Reconstructed X-Ray CT scan of dry cellulose foam. (b) Idealisation of the foam as an assembly of capillary tubes.

macrovoids is clearly seen in the CT scan. Corresponding SEM images have been reported by Mirzajanzadeh et al. [11], and Kim et al. [9]. The macrovoids of this foam are of average diameter 0.5 mm to 3 mm, with microvoids within the cell wall typically of dimension 1 μm to 10 μm . The voids are interconnected, and an idealisation of this material as an assembly of capillary tubes is shown in Figure 3(b).

2.2. Methodology

An inverted U-shaped siphon was made from dry cellulose foam. It connected an upper water Reservoir 1 of initial surface-height $h_1 = 100$ mm to a lower water Reservoir 2 of initial surface height $h_2 = 70$ mm (see Figure 2). The cross-section area of each reservoir was 0.003 m^2 . The siphon was of rectangular cross-section, of dimension 35 mm \times 20 mm. The leftmost arm of the inverted U-tube was of height $H_0 = 37$ mm above the surface of Reservoir 1, and therefore exceeded the Jurin height $h_J = 24$ mm as measured previously by Mirzajanzadeh et al. [11]. The rightmost column was of height $(H_0 + h_1 - h_2) = 67$ mm

above the water level of Reservoir 2.

The experiment began by immersing the bottom of the vertical arms of dry foam simultaneously in the two reservoirs. A CMOS camera (Pixelink) recorded the water level in both reservoirs at a frequency of one frame every 10 s for the first 1000 s, and subsequently at one frame per 1000 s. The reservoirs and siphon were placed inside an airtight PMMA enclosure maintained at room temperature and 99 % relative humidity. A control reservoir (Reservoir 3) was placed inside the PMMA enclosure to measure the rate of water evaporation from the reservoirs into the atmosphere of the enclosure during the experiment; its height h_3 was measured using the same camera as that used for Reservoirs 1 and 2. An additional shallow reservoir provided water vapour to maintain 99 % relative humidity throughout the experiment: a hygrometer monitored the relative humidity and a thermometer measured the temperature. The experiment was repeated twice using nominally identical material and test conditions to show that the results were reliable and reproducible.

2.3. Results and Interpretation

Upon immersion of the inverted U-tube into Reservoirs 1 and 2, water permeated into the foam and wet-fronts rose against gravity along the vertical arms above the water level of the two reservoirs. The wet fronts rose above the Jurin height $h_J = 24$ mm and migrated along the horizontal portion of the inverted U-tube until they met. The clock was started ($t = 0$) when the water fronts met. A continuous discharge of water ensued from Reservoir 1 to Reservoir 2, implying that a siphon discharge was established with pipe flow along the length of the inverted U-tube from the upper Reservoir 1 to the lower Reservoir 2. The water level difference Δh between the reservoirs was recorded as a function of time and denoted

by Δh_0 at $t = 0$.

A plot of h_1 , h_2 , and h_3 versus time t is shown in [Figure 4\(a\)](#) for Test 1. The data suggests that water flow occurs from Reservoir 1 to 2. The height h_3 remains constant throughout the test which proves that the evaporation of water from the reservoirs into the atmosphere of the PMMA enclosure is negligible. The height difference $\Delta h = h_1 - h_2$ is plotted as $\Delta h/\Delta h_0$ versus time t in [Figure 4\(b\)](#) for 3 nominally identical tests (Test 1 - Test 3). The curve fit $\Delta h/\Delta h_0 = \exp(-t/\tau)$ with $\tau = 7.8$ h is included in [Figure 4\(b\)](#) and supports the conclusion that Δh decays exponentially with time.

The exponential decay of $\Delta h(t)$ is consistent with pipe flow along a set of capillaries in the U-tube: the flow rate \dot{Q} , scaling with \dot{h} , is proportional to the fluid head difference Δh . The main conclusion from this critical test is that siphon flow occurs and is driven by the difference in height of the two reservoirs. We conclude that capillary flow continues above $h_J = 24$ mm to prime the siphon. We proceed to give a theoretical framework for capillary flow through the inverted U-tube of foam by assuming that the initial height H_0 dictates the fraction of capillaries that run full between the reservoirs. This theoretical framework is then used to design a set of discharge experiments in order to probe the micromechanics of capillary flow within the foam.

3. Theory of Siphon Discharge

A theory of siphon discharge is now developed by assuming that the U-tube of foam behaves as a set of N parallel capillary tubes. The distribution of the number of capillary tubes is governed by a probability density function $p(a)$ of radius a where

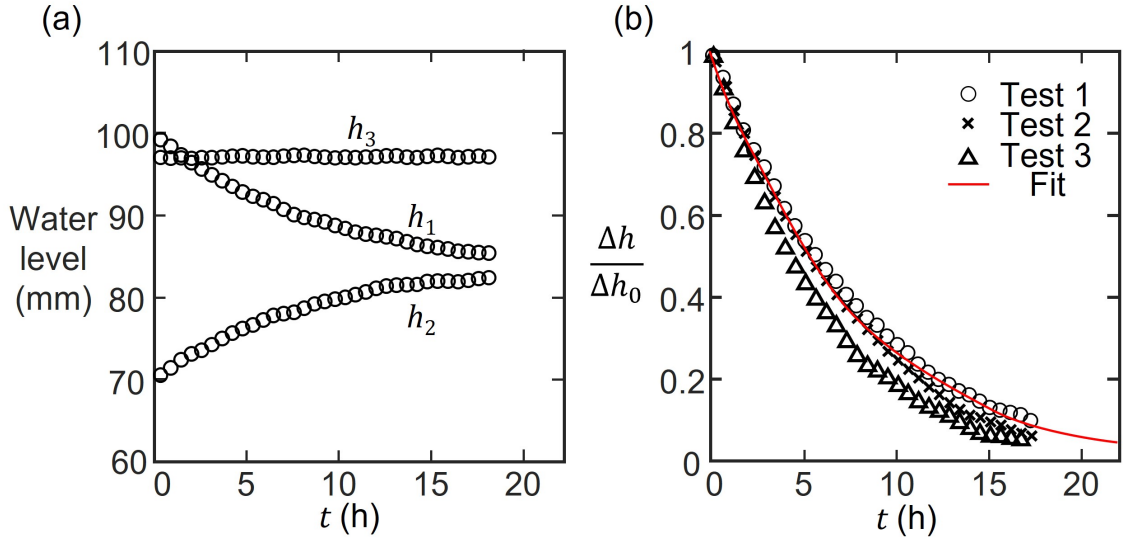


Figure 4: Results of the critical experiment. (a) Temporal variations of the three heights h_1 , h_2 , and h_3 in Test 1; (b) Comparison of responses of 3 nominally identical tests in terms of the temporal variation of the normalised water level difference between the reservoirs.

$$\int_0^\infty p(a) da = 1. \quad (5)$$

We seek $p(a)$ from a suitable set of discharge experiments. To do so, assume that the tubes behave independently with no cross-flow among them. Each tube of radius a self-primes provided that its Jurin height, as given by Equation (4), exceeds H_0 . The flow rate $\dot{q}(a)$ for established pipe flow through each tube equals that of Poiseuille flow. We assume that each tube is of effective length $L = 2H_0 + l + \Delta h_0$ (see schematic in Figure 2) such that L is the arc-length of the foam exposed above water level in the reservoirs. Then recalling that the pressure difference between the ends of the tube is $\rho g \Delta h$, we obtain.

$$\dot{q} = \frac{\pi a^4 \rho g \Delta h}{8 \eta L}. \quad (6)$$

Introduce the cut-off value a_C as the radius of the tube of Jurin height equal to H_0 such

that

$$a_C = \frac{2\gamma'}{\rho g H_0}, \quad (7)$$

Tubes of radius exceeding a_C do not contribute to the flow. Consequently, the total flow rate \dot{Q} is given by

$$\dot{Q} = N \int_0^{a_C} p(a) \dot{q}(a) da. \quad (8)$$

Upon making use of [Equation \(6\)](#), \dot{Q} can also be written in the form

$$\dot{Q} = \frac{\pi \rho g \Delta h}{8\eta L} a_e^4 \quad (9)$$

where we have introduced an overall effective tube radius a_e for the column, as defined by

$$a_e^4 = N \int_0^{a_C} a^4 p(a) da \quad (10)$$

Reservoirs 1 and 2 are of cross-sectional areas A_1 and A_2 , respectively. Then, continuity of flow demands that $\dot{Q} = -A_1 \dot{h}_1 = A_2 \dot{h}_2$, giving

$$\Delta \dot{h} = \dot{h}_1 - \dot{h}_2 = \frac{\dot{Q}}{\hat{A}} \quad (11)$$

where $\hat{A} = A_1 A_2 / (A_1 + A_2)$.

Now eliminate \dot{Q} from [Equation \(9\)](#) by making use of [Equation \(11\)](#), to obtain $\Delta \dot{h}$ in

terms of Δh , with solution

$$\Delta h = \Delta h_0 \exp(-t/\tau) \quad (12)$$

where the time-constant τ is given by

$$\tau = \frac{8\eta\hat{A}L}{\pi\rho g a_e^4} \quad (13)$$

Equation (12) implies that a plot of $-\ln(\Delta h/\Delta h_0)$ versus t is a straight line of slope $(1/\tau)$ for any given values of $(\Delta h_0, H_0)$.

It remains to deduce $p(a)$ and N . To do so, first recall that the critical radius a_C is directly related to H_0 via $a_C = 2\gamma'/(\rho g H_0)$ and is independent of Δh_0 . Consequently, a_e and τ as defined by Equation (10) and Equation (13), respectively, are functions of H_0 , but are independent of Δh_0 . Thus, a set of discharge experiments can be conducted such that τ is measured for selected values of $(\Delta h_0, H_0)$. The value of a_e corresponding to any measured value of τ can be determined via Equation (13), and can be plotted as a function of H_0 for selected values of Δh_0 . A set of experiments are reported in the following section in order to measure the dependence of a_e upon H_0 . But, in order to develop the theory further, it is anticipated that the functional form of $a_e(H_0)$ is

$$a_e = a_m \exp(-\beta H_0) \quad (14)$$

and the value of the constants (a_m, β) are determined by a best fit to the experimental data. Here β is a distribution parameter while a_m is the effective tube radius of the bundle

of N parallel tubes when all tubes contribute to the liquid flow. We proceed to deduce $p(a)$ upon assuming that Equation (14) is an adequate representation for $a_e(H_0)$. First, differentiate both sides of Equation (14) with respect to a_C and make use of Equation (7) to obtain

$$\frac{da_e}{da_C} = \frac{2\beta\gamma'a_m}{\rho ga_C^2} \exp\left(-\frac{\beta'}{a_C}\right) \quad (15)$$

where $\beta' = 2\gamma'\beta/\rho g$.

Then, differentiate both sides of Equation (10) with respect to a_C to obtain

$$4a_e^3 \frac{\partial a_e}{\partial a_C} = Na_C^4 p(a_C) \quad (16)$$

and upon making suitable use of Equation (14) and Equation (15), it follows that

$$Np(a) = \frac{8\beta\gamma'}{\rho ga_m^2} \left(\frac{a_m}{a}\right)^6 \exp\left(-\frac{4\beta'}{a}\right) \quad (17)$$

A slightly more sophisticated functional form of $a_e(H_0)$ comprises the sum of two exponential decay functions, such that Equation (14) is replaced by

$$a_e = a_1 \exp(-\beta_1 H_0) + a_2 \exp(-\beta_2 H_0) \quad (18)$$

in terms of tube radii (a_1, a_2), and two distribution parameters (β_1, β_2). Following the same steps as that used to obtain Equation (17) from Equation (15), Equation (18) leads to

$$Np(a) = \frac{8\gamma'}{\rho g a^6} \left[a_1 \beta_1 \exp\left(\frac{-\beta'_1}{a}\right) + a_2 \beta_2 \exp\left(\frac{-\beta'_2}{a}\right) \right] \times \left[a_1 \exp\left(\frac{-\beta'_1}{a}\right) + a_2 \exp\left(\frac{-\beta'_2}{a}\right) \right]^3 \quad (19)$$

where $\beta'_1 = 2\gamma'\beta_1/\rho g$, and $\beta'_2 = 2\gamma'\beta_2/\rho g$. Finally, the number of capillaries within the specimen N is obtained by substitution of Equation (17) or Equation (19) into the normalisation, Equation (5).

4. Siphon Discharge Experiments

The above theory suggests that the siphon discharge characteristics is given by Equation (12), and the time constant τ scales with H_0 in accordance with Equation (13) and Equation (14). A systematic set of experiments were performed in order to measure $\Delta h(t)$ and τ , and deduce $a_e(H_0)$ to thereby assess the accuracy of this theoretical approach. Specifically, a set of discharge experiments were performed with Δh_0 held fixed at 27 mm, 37 mm, and 57 mm, and H_0 varied from 7.9 mm to 78 mm.

4.1. Results and Discussion

The measured responses $\Delta h(t)$ for selected values of Δh_0 and H_0 are plotted in the form of $\ln(\Delta h(t)/\Delta h_0)$ versus time t in Figure 5. With this choice of axis, the data lay along a series of straight lines of slope $-(1/\tau)$, in support of Equation (12). The results and details of these experiments are summarised in the supplementary Table S1.

The measured values of $1/\tau$ are used to deduce values for a_e via Equation (13), and

the dependence of a_e upon H_0 for the three selected values of Δh_0 is given in [Figure 6\(a\)](#). Note that the data for $a_e(H_0)$ are independent of Δh_0 as anticipated by [Equation \(14\)](#), see [Figure 6\(a\)](#). We conclude that a foam column can be idealised as a set of independent capillary tubes and the value of H_0 dictates the proportion of the tubes that self-prime and run full in the U-shaped siphon. Two best fits to the $a_e(H_0)$ data have been performed, Fit 1 for [Equation \(14\)](#) and Fit 2 for [Equation \(18\)](#). Fit 1 gives $a_m = 918 \text{ }\mu\text{m}$ and $\beta = 0.0415 \text{ mm}^{-1}$. Fit 2 provides $a_1 = 952 \text{ }\mu\text{m}$, $\beta_1 = 0.0606 \text{ mm}^{-1}$, $a_2 = 100 \text{ }\mu\text{m}$, and $\beta_2 = 0.00210 \text{ mm}^{-1}$. Clearly Fit 2 is more accurate, particularly at large values of H_0 , see [Figure 6\(a\)](#). Recall that the probability density functions $p(a)$ can be obtained from [Equation \(17\)](#) and [Equation \(19\)](#) for Fits 1 and 2, respectively, and both functions are plotted in [Figure 6\(b\)](#) assuming $\gamma' = 0.0020 \text{ N/m}$, $\rho = 1000 \text{ kg/m}^3$, and $g = 9.81 \text{ m/s}^2$.

4.2. Density Profile along the Siphon

X-ray CT Scanning was used to obtain density profiles along the foam siphon after interrupting the siphon discharge tests at 89 hours for $H_0 = 60 \text{ mm}$, $\Delta h_0 = 27 \text{ mm}$ and at 42 hours for $H_0 = 60 \text{ mm}$, $\Delta h_0 = 57 \text{ mm}$. The tests were interrupted at the point where the air-exposed lengths of the left vertical arms of both siphons were 70 mm. Additionally, a test was performed such that $H_0 = 15 \text{ mm}$ and $\Delta h_0 = 27 \text{ mm}$. The X-ray CT scan of this test was done 2 hours after the test had started.

The X-ray scans were performed using an 80 kV X-ray source with 130 μA operating current in an industrial X-ray Computed Tomography machine (NIKON XT H 225ST). The working distance of the sample from the X-ray source was such that the dimension of each side of a voxel unit was limited to 90 μm and thereby produces a slice of thickness

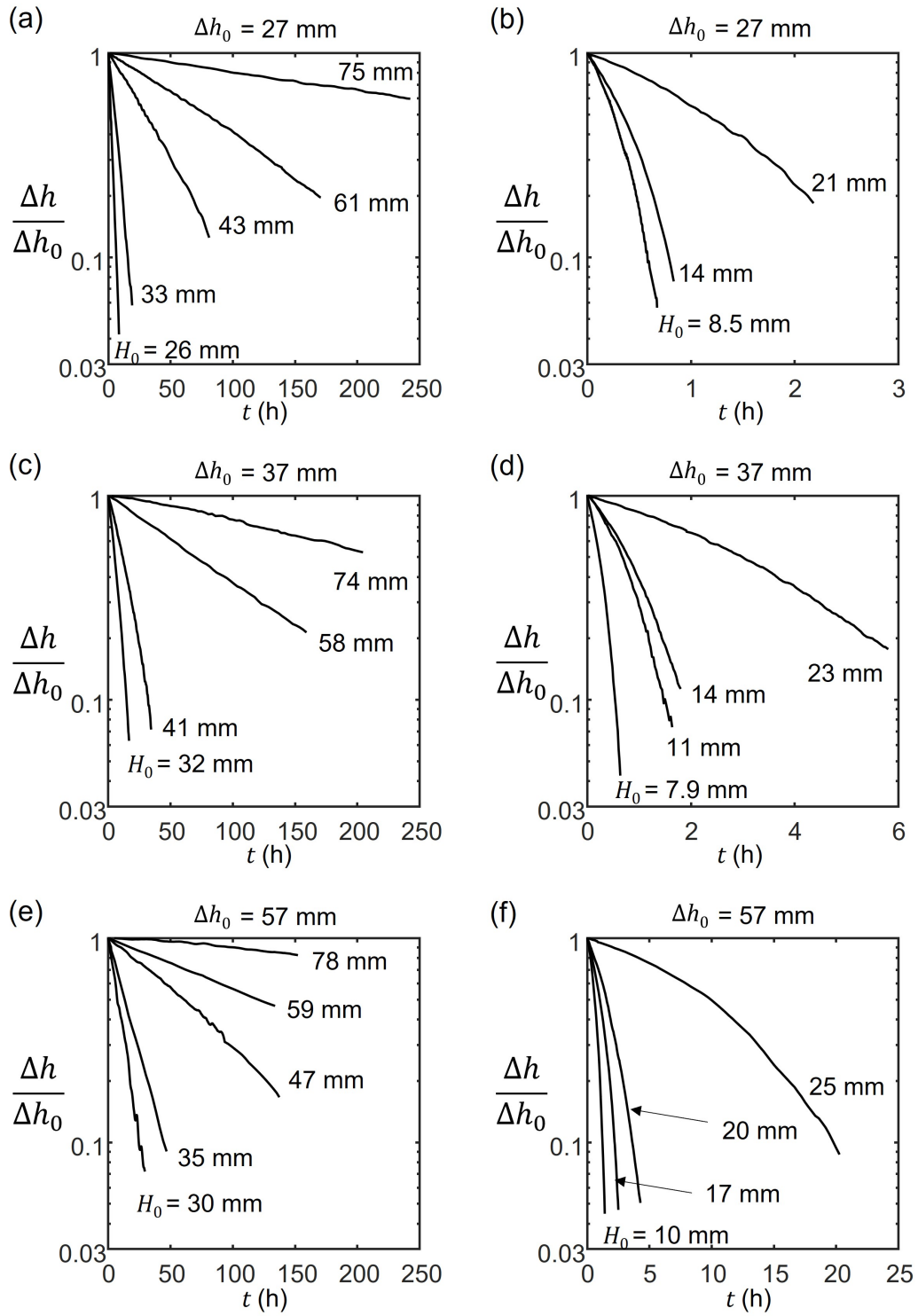


Figure 5: Results of siphon discharge experiments are shown in (a) and (b) for $\Delta h_0 = 27$ mm, in (c) and (d) for $\Delta h_0 = 37$ mm, and in (e) and (f) for $\Delta h_0 = 57$ mm. Selected values of H_0 (mm) are used, such that H_0 range from 78 mm to 26 mm in (a), (c), and (e), and from 25 mm to 7.9 mm in (b), (d), and (f).

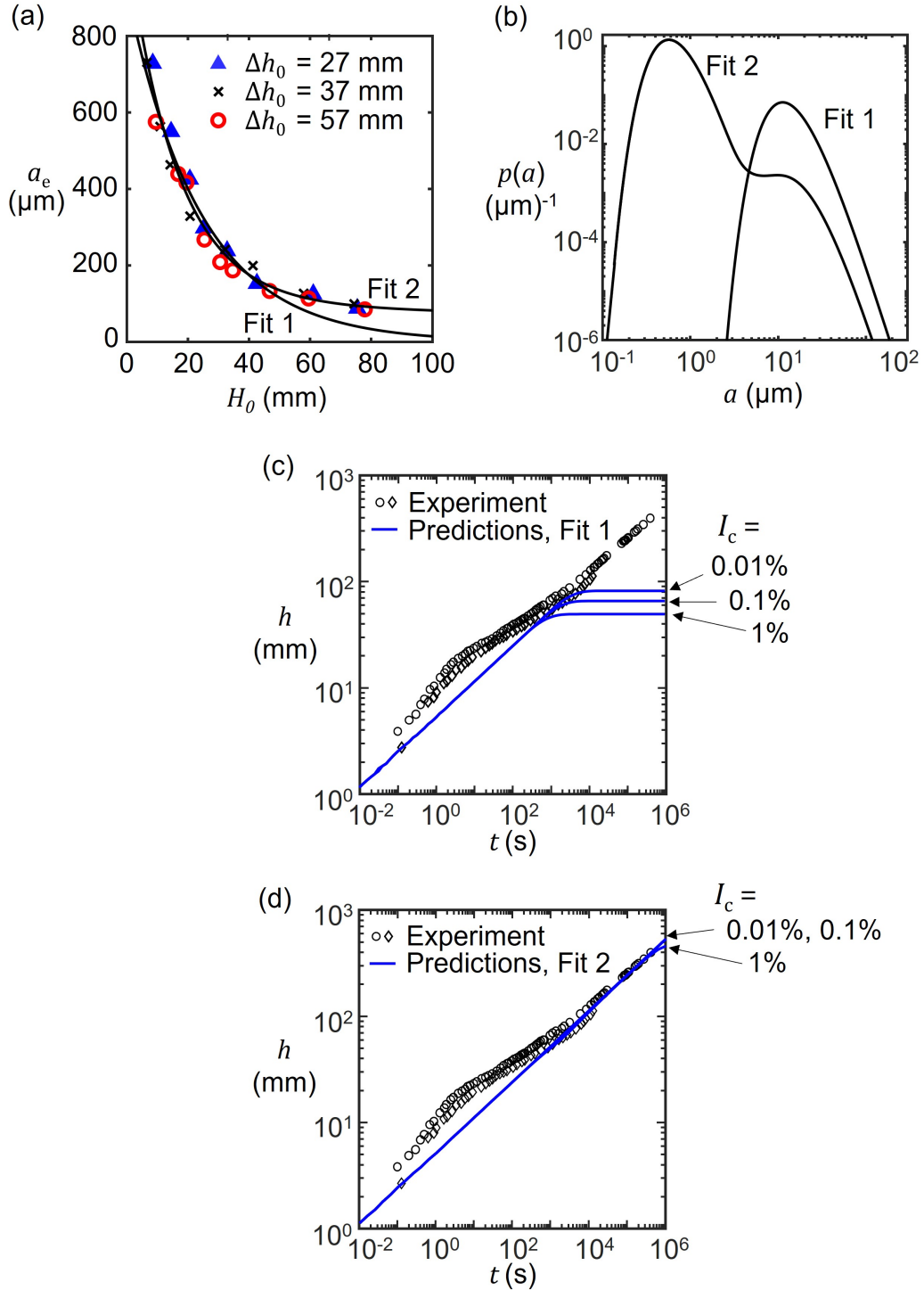


Figure 6: (a) Measured variation of effective siphon radius a_e as a function of siphon height H_0 as deduced from Equation (13). The least square fit of the form $a_e = a_m \exp(-\beta H_0)$ is shown as Fit 1. We find $a_m = 918 \mu\text{m}$ and $\beta = 0.0415 \text{ mm}^{-1}$. The least square fit of the form $a_e = a_1 \exp(-\beta_1 H_0) + a_2 \exp(-\beta_2 H_0)$ is shown as Fit 2. We find $a_1 = 952 \mu\text{m}$, $\beta_1 = 0.0606 \text{ mm}^{-1}$, $a_2 = 100 \mu\text{m}$ and $\beta_2 = 0.00210 \text{ mm}^{-1}$. (b) Predicted $p(a)$ vs a given by Equation (17) for Fit 1, and Equation (19) for Fit 2. (c) and (d) The predicted h vs t plots for a infinite V(RF) test are compared with experimental measurements by Mirzajanzadeh et al. [11].

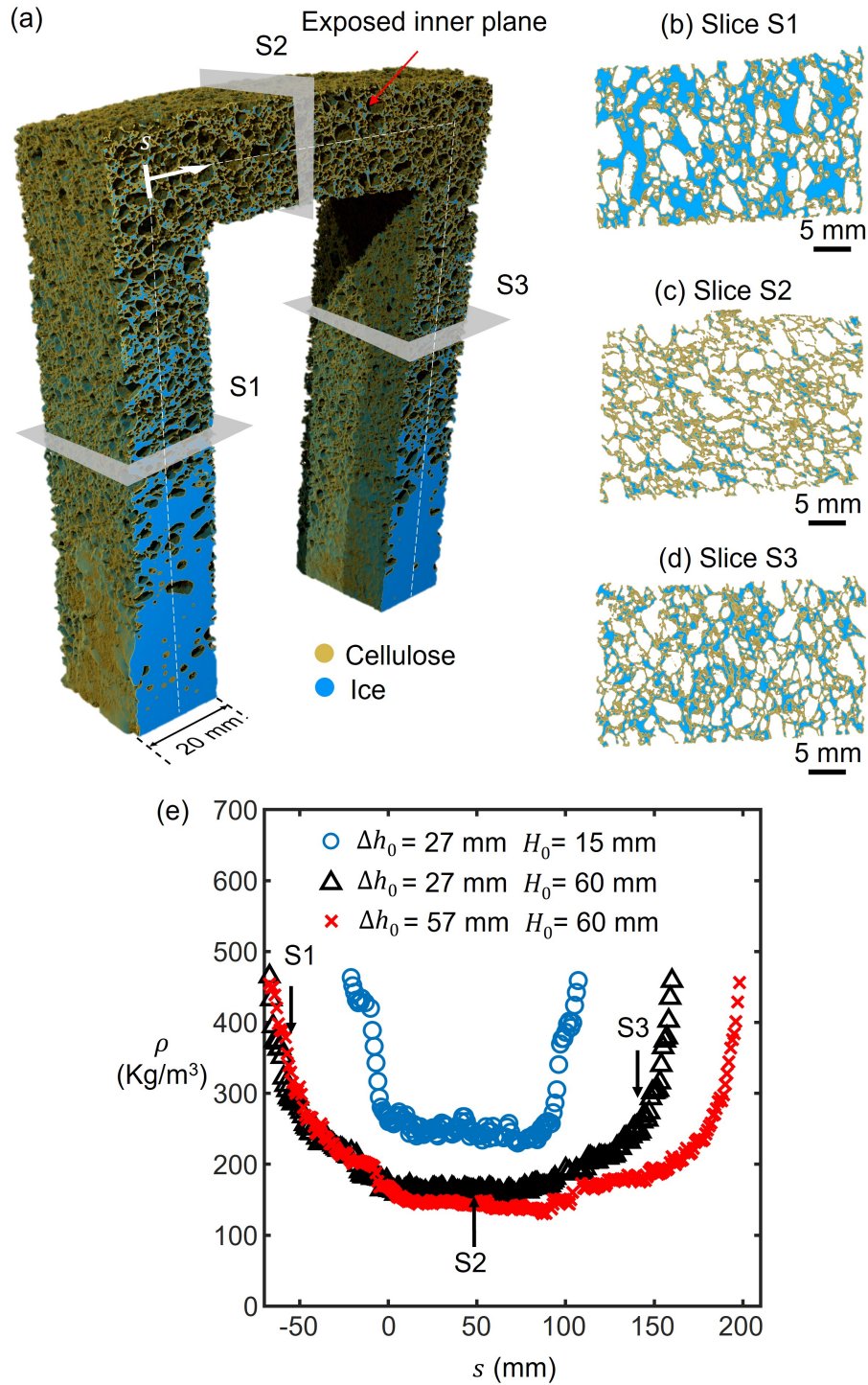


Figure 7: (a) Reconstructed X-Ray CT scan of a frozen wet U-tube foam after interruption of a discharge test at 89 hours. An inner plane of the frozen siphon is shown. s indicates the co-ordinate system that follows the arc of the inverted U-tube. The position $s = 0$ is marked with a thick white line. (b)-(d) shows reconstructed slices (S1, S2, S3) of the foam. (e) Experimentally measured spatial density profile along the length of the wet foam-siphon for 3 different set of $(\Delta h_0, H_0)$.

approximately 90 μm . Each scan took one hour. In order to prevent liquid water migration in the foam during the scan, the wet foam was first frozen after interruption of the test. The procedure was as follows. After interrupting the test, the foam was immediately transferred to an aluminium container submerged in liquid nitrogen and maintained there for 15 minutes to freeze. The temperature inside the aluminium container was $-40\text{ }^{\circ}\text{C}$ to $-50\text{ }^{\circ}\text{C}$. The frozen foam was then transferred to an insulated polystyrene container and suspended over a liquid nitrogen bath during the X-ray scan. The grey-values of the voxels in the reconstructed 3D model was converted to physical densities by using an experimental calibration scheme described in supplementary Section S1. This enabled us to infer an approximate 3D spatial density distribution in the foam. The reconstructed CT Scan of a frozen siphon is shown in [Figure 7\(a\)](#) for $\Delta h_0 = 27\text{ mm}$, and $H_0 = 60\text{ mm}$. The CT Scan is manipulated by a commercial software (VGSTUDIO MAX) to expose an inner plane. Three representative slices are shown in [Figure 7\(b\)](#), (c), and (d) to illustrate the presence of ice in the cell walls of the cellulose foam. The density profile along the siphon was determined by virtually dividing the foam into an array of 2 mm thick slices, with a 1 mm gap between the mid-planes of two consecutive slices. The average density of the voxels contained in each slice was calculated and plotted in [Figure 7\(e\)](#) for the 3 tests.

[Figure 7](#) clearly shows that the effective density of water and cellulose is almost constant along the horizontal arm of the inverted U-tube. This is consistent with the notion that this top portion contains filled capillaries rather than a concentration gradient of water that leads to diffusion. The effective density is insensitive to the value of Δh_0 , but is dependent upon the value of H_0 : less water enters the top of the inverted U-tube with increasing H_0 . Capillary rise is evident within both vertical columns of the inverted U-tube.

5. Prediction of Vertical Capillary Rise in Cellulose Foam

The measured probability density function $p(a)$ from the siphon experiments can be used to make quantitative predictions of capillary flow in other experiments, for example capillary rise in a dry foam. Mirzajanzadeh et al. [11] reported a series of experiments and results for the same cellulose foam as that considered in the present study. The methodology of the experiment was as follows: the bottom face of a dry cellulose foam column was placed in a water reservoir. The length of the foam column was 400 mm with a cross section of dimension 22 mm \times 22 mm. The height of the rising water front h was observed as a function of time. Mirzajanzadeh et al. [11] referred to this type of experiment as a Vertical infinite Reservoir Fed test, with the abbreviation V(RF) test. We proceed to predict time-dependent vertical capillary rise height in a dry cellulose foam column and compare the results with the previously reported experimental observations of Mirzajanzadeh et al. [11].

Capillary rise in a vertical column of dry foam is now analysed, with $t = 0$ denoting the instant when the bottom end of the column is immersed in a water reservoir. The foam is idealised as an array of independent capillaries with probability density function $p(a)$. In the prediction given below, we use the two choices of $p(a)$ as given by Equation (17) and Equation (19). Write y as the vertical co-ordinate such that $y = 0$ is the surface of the reservoir. At time $t > 0$ the water in a representative capillary of radius a has attained a height $h(t, a)$ which is specified by Equation (2).

Next, introduce the function $g(y, t, a)$ such that, for any tube of radius a at time t , $g(y, t, a) = 1$ when $y \leq h(t, a)$ and $g(y, t, a) = 0$ for any other value of y . The function $g(y, t, a)$ can be written as

$$g(y, t, a) = (1 - \mathcal{H}(y - h(t, a))), \quad (20)$$

in terms of the usual Heaviside step function. The water occupancy fraction in the capillary bundle $I(y, t)$ follows as

$$I(y, t) = \frac{\int_0^\infty a^2 p(a) g(y, t, a) da}{\int_0^\infty a^2 p(a) da} \quad (21)$$

$I(y, t)$ is a measure of the degree of water-saturation of the cellulose foam column and lies in the range $0 \leq I(y, t) \leq 1$, such that $I(y, t) = 1$ signifies a fully water-saturated foam and $I(y, t) = 0$ signifies dry foam. It remains to identify the liquid front by setting a threshold cut-off value I_C such that the foam is deemed wet when $I > I_C$. The liquid front of the capillary bundle $h_b(t)$ is set by the identity

$$I(y = h_b, t) = I_C \quad (22)$$

We predict $h_b(t)$ using three cut-off values $I_C = 0.01 \%$, 0.1% , 1% and compare with the data from Mirzajanzadeh et al. [11] in [Figure 6\(c\)](#) and [Figure 6\(d\)](#) for $p(a)$ given by [Equation \(17\)](#) and [Equation \(19\)](#). The predictions are calculated assuming the following values of the other material parameters: $\gamma' = 0.0020$ N/m, $\eta = 0.00089$ m²/s, $\rho = 1000$ kg/m³, and $g = 9.81$ m/s².

We observe from [Figure 6\(c\)](#) that the predictions are in agreement with the experimental observations in the range $40 \text{ mm} < h < 80 \text{ mm}$ and are inaccurate elsewhere. Fit 2 gives the more accurate prediction, see [Figure 6\(d\)](#); excellent agreement with measurements is

obtained except for the regime $3 \text{ mm} < h < 40 \text{ mm}$ where there is a change in slope of the h versus t curve.

6. Conclusions

Direct experimental evidence has been provided to show that capillary liquid transport occurs above the previously identified Jurin height in cellulose foam. The results from the siphon discharge experiments suggest that the dry foam can be idealised as a bundle of capillary tubes with a spectrum of radii a as described by a probability density function $p(a)$. The siphon experiments reveal that the capillary tubes are of radius in the range $1 \text{ }\mu\text{m}$ to $300 \text{ }\mu\text{m}$, consistent with the notion of capillary flow through the micropores in the cellulose cell wall. X-ray CT scan images of selected wet inverted U-shaped foam siphon support this conclusion.

Washburn's vertical capillary rise kinematics is used for each idealised capillary to predict the water rise in a dry cellulose foam as idealised by a parallel array of capillary tubes. The degree to which cross-flow between neighbouring capillary tubes influences fluid migration in the foam remains a topic for future work.

Acknowledgement

The authors are grateful for financial support from the European Research Council in the form of an Advanced Grant (MULTILAT, 669764).

References

- [1] M. Sahimi, G. R. Gavalas, T. T. Tsotsis, Statistical and continuum models of fluid-solid reactions in porous media, *Chemical Engineering Science* 45 (1990) 1443–1502.
- [2] M. O. Adebajo, R. L. Frost, J. T. Kloprogge, O. Carmody, S. Kokot, Porous materials for oil spill cleanup: a review of synthesis and absorbing properties, *Journal of Porous materials* 10 (2003) 159–170.
- [3] J. S. A. Cortez, B. I. Kharisov, T. E. S. Quezada, T. C. H. García, Micro-and nanoporous materials capable of absorbing solvents and oils reversibly: the state of the art, *Petroleum Science* 14 (2017) 84–104.
- [4] J. Ge, H. Y. Zhao, H. W. Zhu, J. Huang, L. A. Shi, S. H. Yu, Advanced sorbents for oil-spill cleanup: recent advances and future perspectives, *Advanced materials* 28 (2016) 10459–10490.
- [5] C. Carrell, A. Kava, M. Nguyen, R. Menger, Z. Munshi, Z. Call, M. Nussbaum, C. Henry, Beyond the lateral flow assay: A review of paper-based microfluidics, *Microelectronic Engineering* 206 (2019) 45–54.
- [6] T. H. Gilman, Absorbent foam wound dressing, 2004. US Patent 6,787,682.
- [7] M. Märtson, J. Viljanto, T. Hurme, P. Laippala, P. Saukko, Is cellulose sponge degradable or stable as implantation material? an in vivo subcutaneous study in the rat, *Biomaterials* 20 (1999) 1989–1995.
- [8] M. Mirzajanzadeh, V. S. Deshpande, N. A. Fleck, The swelling of cellulose foams due to liquid transport, *Journal of the Mechanics and Physics of Solids* 136 (2020) 103707.
- [9] J. Kim, J. Ha, H. Y. Kim, Capillary rise of non-aqueous liquids in cellulose sponges, *Journal of Fluid Mechanics* 818 (2017).
- [10] H. Y. Kim, L. Mahadevan, Capillary rise between elastic sheets, *Journal of Fluid mechanics* 548 (2006) 141–150.
- [11] M. Mirzajanzadeh, V. S. Deshpande, N. A. Fleck, Water rise in a cellulose foam: By capillary or diffusional flow?, *Journal of the Mechanics and Physics of Solids* 124 (2019) 206–219.
- [12] A. Raina, V. S. Deshpande, N. A. Fleck, Analysis of electro-permeation of hydrogen in metallic alloys, *Philosophical Transactions of the Royal Society A: Mathematical, Physical and Engineering Sciences* 375 (2017) 20160409.
- [13] A. Raina, V. S. Deshpande, N. A. Fleck, Analysis of thermal desorption of hydrogen in metallic alloys, *Acta Materialia* 144 (2018) 777–785.
- [14] E. W. Washburn, The dynamics of capillary flow, *Physical review* 17 (1921) 273.

- [15] J. M. Bell, F. Cameron, The flow of liquids through capillary spaces, *The Journal of Physical Chemistry* 10 (1906) 658–674.
- [16] R. Lucas, Ueber das zeitgesetz des kapillaren aufstiegs von flüssigkeiten, *Kolloid-Zeitschrift* 23 (1918) 15–22.
- [17] J. Jurin, ii. an account of some experiments shown before the royal society; with an enquiry into the cause of the ascent and suspension of water in capillary tubes., *Philosophical Transactions of the Royal Society of London* 30 (1718) 739–747.
- [18] R. Rye, F. Yost, J. Mann, Wetting kinetics in surface capillary grooves, *Langmuir* 12 (1996) 4625–4627.
- [19] L. Romero, F. Yost, Flow in an open channel capillary, *Journal of Fluid Mechanics* 322 (1996) 109–129.
- [20] J. Mann Jr, L. Romero, R. Rye, F. Yost, Flow of simple liquids down narrow ssv grooves, *Physical Review E* 52 (1995) 3967.
- [21] N. Ichikawa, K. Hosokawa, R. Maeda, Interface motion of capillary-driven flow in rectangular microchannel, *Journal of colloid and interface science* 280 (2004) 155–164.
- [22] D. Yang, M. Krasowska, C. Priest, M. N. Popescu, J. Ralston, Dynamics of capillary-driven flow in open microchannels, *The Journal of Physical Chemistry C* 115 (2011) 18761–18769.
- [23] J. Siddique, D. Anderson, A. Bondarev, Capillary rise of a liquid into a deformable porous material, *Physics of Fluids* 21 (2009) 013106.
- [24] J. Ha, J. Kim, Y. Jung, G. Yun, D. N. Kim, H. Y. Kim, Poro-elasto-capillary wicking of cellulose sponges, *Science advances* 4 (2018) eaao7051.
- [25] S. Wu, H. Yang, G. Xiong, Y. Tian, B. Gong, T. Luo, T. S. Fisher, J. Yan, K. Cen, Z. Bo, K. K. Ostrikov, Spill-SOS: Self-Pumping Siphon-Capillary Oil Recovery, *ACS Nano* 13 (2019) 13027–13036.
- [26] L. Zhao, H. Yang, F. He, Y. Yao, R. Xu, L. Wang, L. He, H. Zhang, S. Li, F. Huang, Biomimetic N-doped sea-urchin-structured porous carbon for the anode material of high-energy-density potassium-ion batteries, *Electrochimica Acta* 388 (2021) 138565.
- [27] N. M. Reis, S. H. Needs, S. M. Jegouic, K. K. Gill, S. Sirivisoot, S. Howard, J. Kempe, S. Bola, K. Al-Hakeem, I. M. Jones, T. Prommool, P. Luangaram, P. Avirutnan, C. Puttikhunt, A. D. Edwards, Gravity-Driven Microfluidic Siphons: Fluidic Characterization and Application to Quantitative Immunoassays, *ACS Sens.* 6 (2021) 4338–4348.
- [28] R. Coda, A study of cellulose based biodegradable foams and sponges, Ph.D. thesis, Georgia Institute of Technology, 2005.

The Transport of Water in a Cellulose Foam

Ratul Das^a, Vikram S. Deshpande^a, Norman A. Fleck^{a,*}

^a*Engineering Department, Cambridge University, Trumpington Street, Cambridge, CB2 1PZ, , England*

Experiment Set A: $\Delta h_0 = 27$ mm					Experiment Set B: $\Delta h_0 = 37$ mm				
Test	H_0 (mm)	τ (h)	a_e (μm)	A_1/A_2	Test	H_0 (mm)	τ (h)	a_e (μm)	A_1/A_2
A1	75	505	87.7	1	B1	74	308	99.5	1
A2	61	105	125	1	B2	58	103	127	1
A3	43	41.2	153	1	B3	41	14.6	199	1
A4	33	6.02	238	1	B4	32	5.96	242	1
A5	26	2.73	298	1	B5	23	3.31	329	7
A6	21	1.10	426	7	B6	14	0.83	463	14
A7	14	0.36	550	7	B7	11	0.66	563	14
A8	8.5	0.21	728	14	B8	7.9	0.21	731	7

Experiment Set C: $\Delta h_0 = 57$ mm

Test	H_0 (mm)	τ (h)	a_e (μm)	A_1/A_2
C1	78	631	84.8	1
C2	59	174	113	1
C3	47	82.2	133	1
C4	35	19.4	187	1
C5	30	11.9	209	1
C6	25	8.84	268	7
C7	20	1.41	417	7
C8	17	1.11	440	7
C9	10	0.66	576	7

Table S1: Summary of results from siphon discharge experiments.

S1. Density Calibration of CT Scans of Wet Frozen Cellulose Foam

An industrial X-Ray Computed Tomography machine (NIKON XT H 225ST) was used to scan the frozen wet foam-siphons. The reconstructed 3D scans of the siphons were an

*Corresponding author

Email address: naf1@cam.ac.uk (Norman A. Fleck)

assembly of numerous voxels of size $90 \mu\text{m} \times 90 \mu\text{m} \times 90 \mu\text{m}$. During the reconstruction process, each voxel was assigned a greyvalue (0 to 255) which was a function of the material density of the voxel. There exists no known standard calibration method to relate the voxel's greyvalue to the physical density for the said X-Ray machine. So, we developed a calibration method for this experiment.

We scanned 7 wet foam samples of known densities (56 kg/m^3 to 616 kg/m^3) and plotted the average greyvalue of the voxels of each sample against the known real physical density to construct an experimental calibration curve. The sample preparation and scanning procedure is as follows. 7 identical cellulose foam pieces of dimension $20 \text{ mm} \times 20 \text{ mm} \times 25 \text{ mm}$ were homogeneously wet to different degrees by adding pre-calculated mass of distilled water. The wet samples are then wrapped in a Low density poly-ethylene (LDPE) bags to stop water evaporation. The wet samples were frozen by submerging them in liquid nitrogen and scanned. The X-Ray scans were done using a 80 kV X-Ray source with $130 \mu\text{A}$ operating current. The working distance of the sample from the X-Ray source was such that the dimension of each side of a voxel unit is $90 \mu\text{m}$. These exact same operating conditions were used for all X-Ray scans in this work. The reconstructed 3D scans were then analyzed using VGSTUDIO MAX software. The averaged greyscale values of all the voxels in each wet foam sample was calculated and plotted against the real average density of the corresponding wet foam. The experimental data is shown in [Table S2](#) and the plot is shown in [Figure S1](#). We then calculated the linear best-fit line which is the required calibration curve. Let D represent real physical density and G represent the greyvalue. Then we can write

$$D = mG + c \tag{1}$$

where $m = 32.4 \text{ kg/m}^3$ and $c = -29.6 \text{ kg/m}^3$

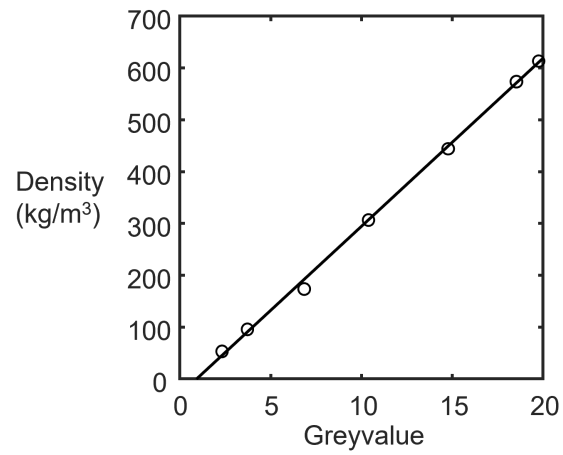


Figure S1: Density calibration of frozen foam in CT scan machine.

Test	Density (kg/m ³)	Greyvalue
F1	56	2.4
F2	98	3.8
F3	176	6.9
F4	309	10
F5	447	15
F6	576	19
F7	616	20

Table S2: Summary of foam densities and corresponding greyvalues.